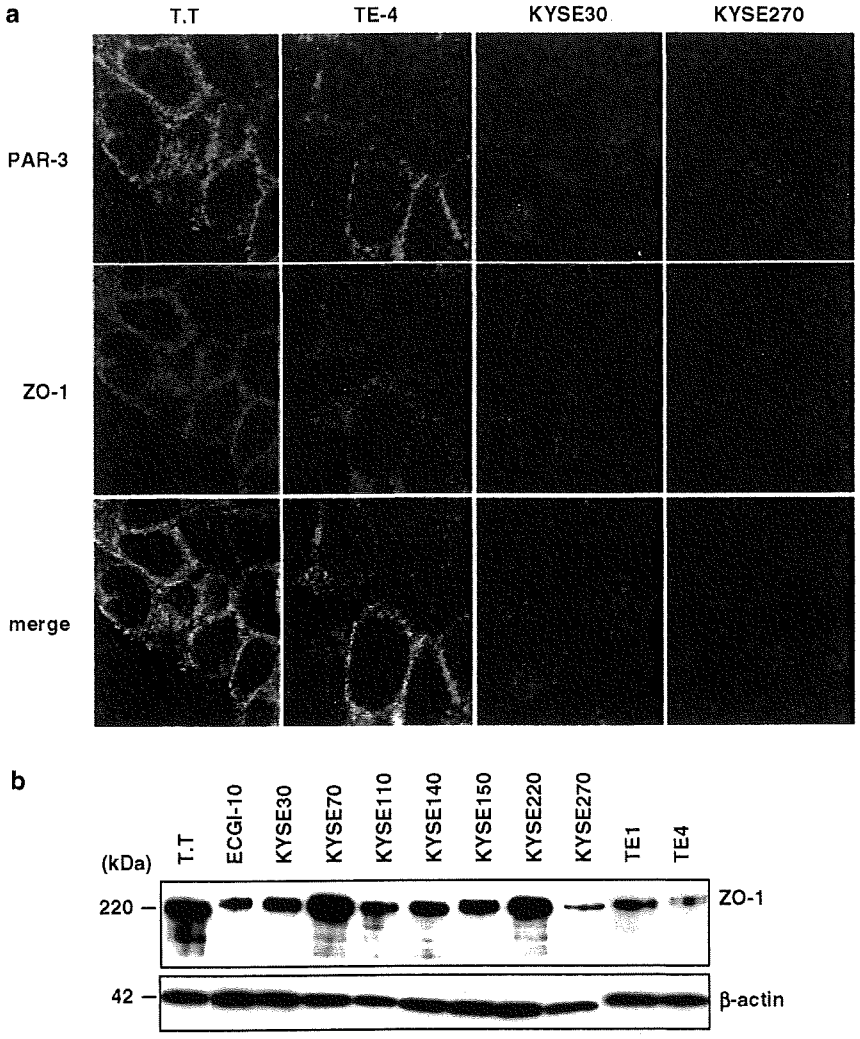

Figure 3 Effect of *PARD3* deletion on the subcellular localization of ZO-1. (**a**) Subcellular localization of PAR-3 and ZO-1 in PAR-3-expressing (T.T, TE-4) and non-expressing (KYSE30, KYSE270) cells. The cells were doubly stained with anti-PAR-3 (green) and anti-ZO-1 (red), and were viewed with a confocal laser scanning microscope. PAR-3 and ZO-1 colocalized at cell cell borders in the T.T and TE-4 cells. The nuclear staining observed with anti-PAR-3 in the KYSE30 and KYSE270 cells is probably nonspecific because of the absence of *PARD3*. Original magnifications, × 1000. (**b**) Immunoblotting analyses of ZO-1 and β-actin, used as an internal control, in 11 ESCC cell lines.

Immunocytochemistry showed that, in addition to a diffuse staining, PAR-3 could now be detected in a linear manner at cell–cell borders in the *PARD3*-transfected KYSE30 and KYSE270 cells, in which it colocalized with ZO-1 (Figure 4b). Transfection of *PARD3* led to a stronger staining of ZO-1 at sites of cell–cell contact compared with control-transfected cells (Figure 4b). This was despite the fact that the total level of ZO-1 was the same in *PARD3* and control transfectants (Figure 4c). Knockdown of the *PARD3* expression in T.T cells was carried out using RNA interference (RNAi). After treatment of T.T cells with small interfering RNA (siRNA) targeting *PARD3*, we observed a decrease in the PAR-3 protein level relative to that observed for cells receiving negative control siRNA, transfection agent alone or left untreated (Figure 4a). Suppression of the PAR-3 expression by siRNA caused a disruption of localization of ZO-1 at cell–cell borders (Figure 4b), although the total level of ZO-1 was unchanged (Figure 4c). Taken together, these findings suggest that PAR-3 promotes the recruitment of ZO-1 to sites of cell–cell contact.

PAR-3 and cell migration

To investigate the role of PAR-3 in cell motility, we performed a monolayer wound-healing assay in knockdown T.T cells. Knockdown of the *PARD3* expression was conducted as described above. Wound closure was shown to be unchanged among *PARD3* siRNA-treated cells, negative control siRNA-treated cells and untreated cells (Supplementary Figure S2).

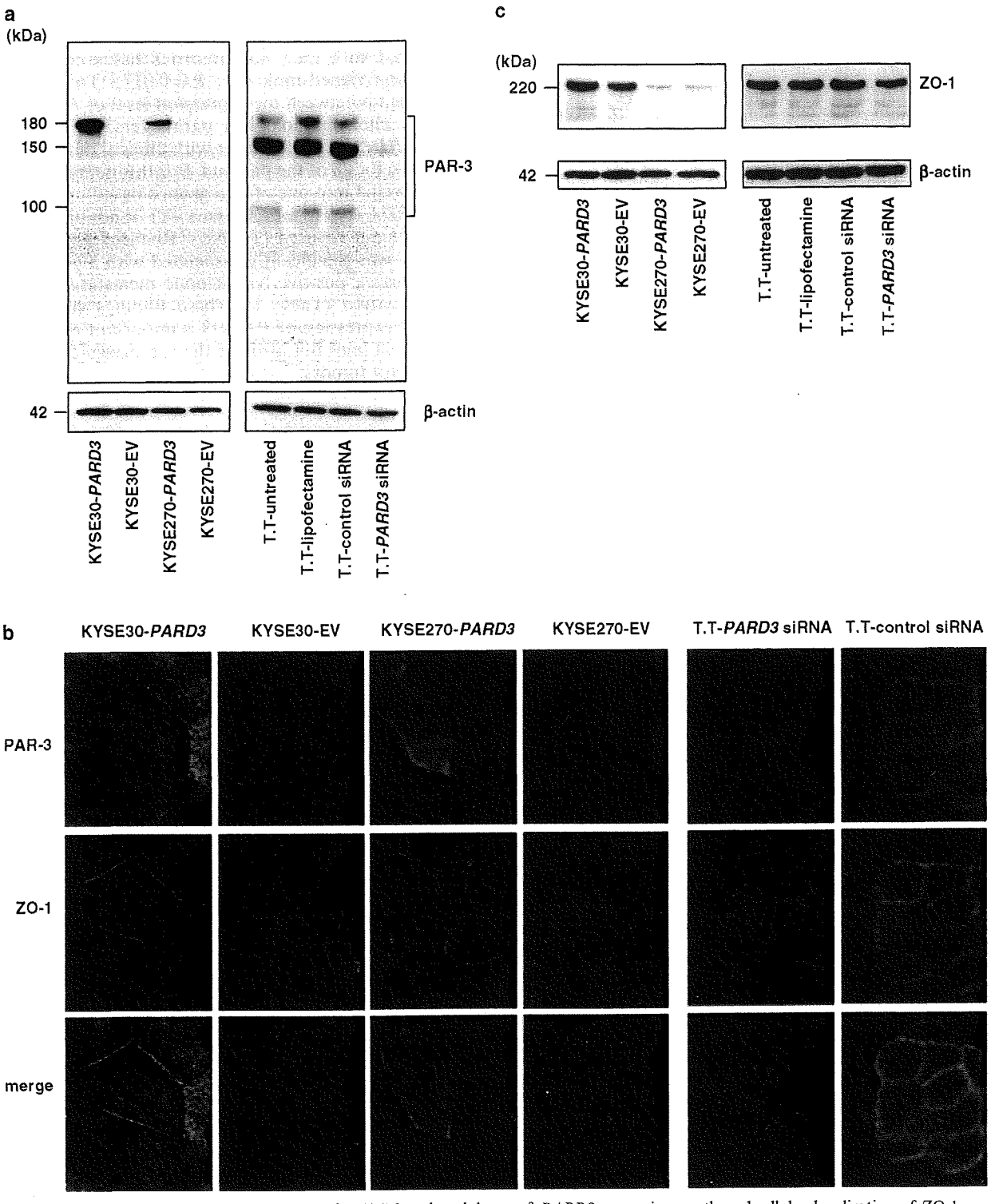

Figure 4 Effect of enforced expression of *PARD3* or knockdown of *PARD3* expression on the subcellular localization of ZO-1. KYSE30 and KYSE270 cells were transfected with the *PARD3* expression vector or with an empty vector (EV). T.T cells were treated with siRNA targeting *PARD3*, control siRNA, transfection agent (lipofectamine) alone or left untreated. (**a**) Immunoblot analysis of PAR-3. Analysis of β-actin served as an internal control. (**b**) Subcellular localization of PAR-3 and ZO-1 in transiently transfected cells. The cells were doubly stained with anti-PAR-3 (green) and anti-ZO-1 (red), and were viewed with a confocal laser scanning microscope. Original magnification, × 1000. (**c**) Immunoblot analyses of ZO-1 and an internal control, β-actin.

This suggests that the suppression of PAR-3 may not affect cell migration.

Analysis of PARD3 *defects in primary tumors*

To determine whether the loss of *PARD3* observed in KYSE30 and KYSE270 carcinoma cell lines was relevant to primary carcinomas in humans, we first determined the DNA copy number of *PARD3* in 40 primary ESCC tumors (Figure 5a). For this analysis, the values were normalized such that the copy number in genomic DNA derived from normal lymphocytes was given a value of 1. Copy number changes were counted as losses if the results of the analysis for a given ESCC tumor were <0.7 (Berggren *et al.*, 2003). Using these parameters, a copy number loss of *PARD3* was observed in 6 (15%) of the 40 tumors.

We then further quantified the mRNA levels of *PARD3* in the available paired tumor and nontumor tissues from 33 ESCC patients (Figure 5b). Patient and tumor characteristics are summarized in Supplementary Table S2. The expression of *PARD3* mRNA was significantly reduced in 23 (70%) of the 33 tumors when compared with their nontumorous tissue counterparts (Wilcoxon signed-rank test, $P=0.017$). To clarify the relationship between the expression level of *PARD3* and various clinicopathological parameters, we correlated the *PARD3* expression level with clinical data that was available for 28 of the patients. For this purpose, tumors were divided into one of two groups based on reduction in *PARD3* levels: tumor tissue (T) <nontumor tissue (NT), or not reduced (T≥NT). Reduced expression of *PARD3* was significantly associated with a younger age (≤65 years), positive lymph node metastasis and poor differentiation (Table 1). These findings suggest that reduced expression of *PARD3* is important not only for cancer cell lines but also for the tumorigenic properties of primary tumors.

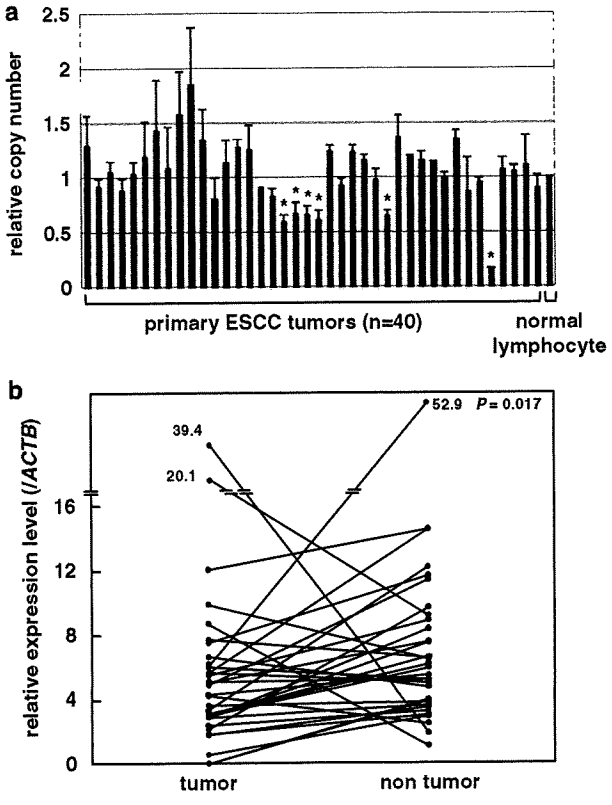

Figure 5 Copy number and expression level of *PARD3* in primary ESCC tumors. (**a**) The copy number of *PARD3* in each of 40 primary ESCC tumors was determined as described in Figure 2a. Values are represented as the mean ± s.d. of three independent experiments. Asterisks indicate tumors with a loss (<0.7) of *PARD3*. The copy number of normal lymphocytes served as a control. (**b**) The relative expression of *PARD3* in paired tumor (T) and nontumor tissues (NT) from 33 patients with primary ESCCs was determined as described in Figure 2b. *P*-values of <0.05 were considered significant.

Discussion

Homozygous deletions have been useful in the positional cloning of a number of tumor suppressor

Table 1 Relationship between clinicopathological features and levels of expression of *PARD3* in 28 primary ESCCs

Characteristics	*PARD3*		P-*value*[a]
	T<NT (n=*18*)	*T≥NT* (n=*10*)	
Age (years)			
≤65	11	2	0.037
>65	7	8	
Gender			
Male	14	8	0.891
Female	4	2	
Tumor diameter (cm)			
≤3 cm	6	7	0.062
>3 cm	12	3	
Stage			
I/II	8	7	0.194
III/IV	10	3	
T classification			
T1/T2	8	7	0.194
T3/T4	10	3	
N status			
N0	5	7	0.031
N1	13	3	
M status			
M0	15	10	0.172
M1	3	0	
Histological differentiation			
Well/moderate	11	10	0.023
Poor	7	0	

Abbreviations: ESCC, esophageal squamous cell carcinoma; NT, nontumor tissue; T, tumor tissue.
[a]χ^2-Test.

genes (Friend *et al.*, 1986; Kamb *et al.*, 1994; Hahn *et al.*, 1996; Li *et al.*, 1997). A putative tumor suppressor is believed to lie on the chromosomal region 10p in ESCC (Aoki *et al.*, 1994). In this study, using high-density SNP arrays, we identified a novel homozygous deletion at the chromosomal region 10p11 in 2 out of 20 ESCC cell lines. Subsequent detailed analyses narrowed down the extent of the shortest region of overlap of the homozygous deletions to exons 3–22 of the gene *PARD3*. Recently, homozygous deletion of *PARD3* has been reported in two lung cancer cell lines (Nagayama *et al.*, 2007).

A few studies have suggested an association of *PARD3* with tumors (Fang and Xu, 2001; Zitzelsberger *et al.*, 2004), and *PARD3* was reported to be amplified in radiation-transformed neoplastic retinal pigment epithelial cell lines (Zitzelsberger *et al.*, 2004). Also, various splicing transcripts of *PARD3* are expressed in primary hepatocellular carcinomas, and the expression of exon 17b deleted *PARD3* variants is downregulated in these carcinomas compared with the surrounding nontumorous liver tissues (Fang and Xu, 2001). However, the biological function of *PARD3* and its clinical significance for cancer are poorly understood. In this study, a gain of *PARD3* copy number (defined as twice the level of normal DNA) was observed in only 1 of the 20 ESCC cell lines tested (TE4 cells) and in none of the 40 primary ESCC tumors analysed. Conversely, a loss of *PARD3* was detected in 15% of the primary ESCC tumors examined, and a reduced expression of *PARD3* mRNA was found in primary ESCC tumors compared with their nontumorous counterparts. The reduced expression of *PARD3* was associated with aggressive ESCC phenotypes, such as positive lymph node metastasis and poor differentiation. To validate these results at the protein level, we unsuccessfully tried to carry out the immunohistochemical analysis of PAR-3 on formalin-fixed and paraffin-embedded sections of primary ESCC specimens. We assume that the anti-PAR-3 antibody is not suitable for formalin-fixed and paraffin-embedded sections. Further studies in more numerous primary samples and studies using immunohistochemistry are needed to determine the clinical importance of PAR-3 in ESCC.

PAR-3 has been implicated in the formation of normal tight junctions at epithelial cell–cell contacts (Joberty *et al.*, 2000; Macara, 2004; Chen and Macara, 2005; Suzuki and Ohno, 2006). PAR-3 plays the role of a scaffold in the recruitment of proteins, such as PAR-6 or aPKC, that are involved in the formation of these junctions (Assémat *et al*, 2008). In agreement with these data, our immunocytochemical analyses showed that PAR-3 colocalized with the tight junction component, ZO-1, at sites of cell–cell contact in T.T and TE-4 cells that express *PARD3*. Unexpectedly, ZO-1 was weakly detected at sites of cell–cell contact in KYSE30 cells that lack *PARD3*. On the other hand, ZO-1 was barely detected in KYSE270 cells, which also lack *PARD3*. Exogenous expression of *PARD3* resulted in the recruitment of ZO-1 to sites of cell–cell contact in KYSE30 and KYSE270 cells without affecting the expression level of ZO-1. Conversely, knockdown of *PARD3* in T.T cells that express this gene caused a disruption of localization of ZO-1 at cell-cell borders. Taken together, these findings suggest that PAR-3 promotes the recruitment of ZO-1 to sites of cell–cell contact, although it may not always be essential for this localization of ZO-1. The finding that *PARD3* affects the formation of tight junction in ESCC cells might partially explain the observed association between the reduced expression of *PARD3* and positive lymph node metastasis, and between poor differentiation of primary ESCCs. However, our wound-healing assay did not show any effect of PAR-3 on cell migration. Further functional studies are needed to determine the implication of PAR-3 in ESCC invasion and metastasis.

Our finding that PAR-3 is important, but not essential, for tight junction formation and ZO-1 recruitment are in partial agreement with previous observations. The targeted disruption of the mouse PAR-3 gene (*Pard3*) results in embryonic lethality with defective epicardial development (Hirose *et al.*, 2006). *Pard3*-deficient epicardial progenitor cells do not form epicardial cysts from which the epicardium is derived. These cells show defects in the localization of PAR-6 and aPKC to the apical domain, but a normal localization of ZO-1 to cell–cell junctions. Interestingly, not all epithelial cells are affected in the *Pard3*-deficient embryo, which may be due to the proposed functional redundancy of PAR-3 and the PAR-3-related protein PAR-3L/PAR-3β (Gao *et al.*, 2002; Kohjima *et al.*, 2002). The function of PAR-3 has also been examined in MDCK II canine epithelial cells (Chen and Macara, 2005). In that study, withdrawal of calcium from the medium caused rapid loss of cell–cell junctions, which could be reversed by the re-addition of calcium (a calcium switch experiment). The normal relocalization of tight junction components at cell–cell contacts within 30 min after re-addition of calcium was profoundly delayed in cells lacking PAR-3, although tight junctions could eventually form even without re-expression of PAR-3.

The exact mechanism by which PAR-3 modulates tight junctions and contributes to tumorigenicity remains to be elucidated. Besides PAR-6 and aPKC, PAR-3 also interacts with other proteins such as 14-3-3, LIMK2 and the Rac-specific guanine nucleotide exchange factor STEF/Tiam1 (Humbert *et al.*, 2006; Assémat *et al.*, 2008). Moreover, recent studies have shown that the PAR-3–PAR-6–aPKC complex associates with the tumor suppressor VHL (von Hippel–Lindau protein) or with PTEN (phosphatase and tensin homologue deleted on chromosome ten) (Wodarz and Näthke, 2007), suggesting potential mechanisms by which PAR-3 might modulate tumorigenicity. Although the mechanism of PAR-3 function in tumors remains to be elucidated and the findings must be verified in a larger sample number, the data presented in this work clearly suggest a role for PAR-3 deletion in the tumorigenesis of ESCC.

Materials and methods

Cell lines and primary tumors

The ESCC cell lines TE-1, TE-5, TE-9, TE-15 and EC-GI-10 were obtained from RIKEN Bioresource Center (Tsukuba, Japan); T.T, T.Tn, KYSE30, KYSE70, KYSE110, KYSE140, KYSE150, KYSE220 and KYSE270 were from Japan Health Sciences Foundation (Osaka, Japan); and TE-4, TE-6, TE-8, TE-10, TE-11 and TE-14 were from Cell Resource Center for Biomedical Research, Tohoku University (Sendai, Japan). All cell lines were maintained in Dulbecco's modified Eagle's medium supplemented with 10% fetal bovine serum. Genomic DNA was isolated from the cell lines with the DNeasy Mini Kit (Qiagen, Tokyo, Japan).

Paired tumor and nontumor tissues were obtained during upper gastrointestinal endoscopic inspection from 40 ESCC patients who underwent biopsy for diagnostic purposes at the Hospital of Kyoto Prefectural University of Medicine (Kyoto, Japan). All biopsy specimens were immediately frozen in liquid nitrogen and stored at −80 °C until required. Genomic DNA and total RNA were isolated from primary samples with the AllPrep DNA/RNA Mini Kit (Qiagen). All tumor samples were available for DNA analyses, and 33 paired tumor and nontumor samples were available for mRNA analyses. Before the study, informed consent was obtained and the study was approved by ethics committees.

Array analysis

Array analyses were carried out with the GeneChip Mapping 250K Sty array (Affymetrix, Santa Clara, CA, USA) according to the manufacturer's instructions. In brief, 250 ng of genomic DNA was digested with a restriction enzyme (*Sty*I), ligated to an adaptor and amplified by PCR. Amplified products were fragmented, labeled by biotinylation and hybridized to the microarrays. Hybridization was detected by incubation with streptavidin–phycoerythrin conjugates, followed by scanning of the array, and analysis was carried out as described earlier (Kennedy *et al*., 2003). Copy number changes were calculated using the Copy Number Analyzer for Affymetrix GeneChip Mapping Arrays (CNAG; http://www.genome.umin.jp; Nannya *et al*., 2005).

PCR analysis

Conventional PCR was performed using Ex Taq DNA Polymerase (Takara, Otsu, Japan) as described by the manufacturer. Genomic DNA and mRNA were quantified with a real-time fluorescence detection method as described earlier (Inagaki *et al*., 2008). Total RNA derived from normal human esophageal epithelial cells was purchased from Ambion (Austin, TX, USA). Single-stranded cDNAs were generated from total RNAs using QuantiTect Reverse Transcription Kit (Qiagen). Primers used for genomic PCR and RT–PCR are listed in Supplementary Table S1. Endogenous controls for mRNA and genomic DNA levels were *ACTB* and the long interspersed nuclear element 1 (LINE-1) (Zhao *et al*., 2004), respectively.

Immunoblotting

Immunoblots were prepared according to the previously reported methods (Yasui *et al*., 2001). Cell lysates (20 μg protein per sample) were separated by SDS–polyacrylamide gel electrophoresis using 10% acrylamide gels. The anti-PAR-3 polyclonal antibody was obtained from Upstate Biotechnology (Lake Placid, NY, USA), the anti-β-actin monoclonal antibody from Sigma-Aldrich (Tokyo, Japan) and the anti-ZO-1 monoclonal antibody from Zymed (South San Francisco, CA, USA). The anti-PAR-3, anti-ZO-1 and anti-β-actin antibodies were used for immunoblotting at dilutions of 1:500, 1:250 and 1:5000, respectively. For secondary immunodetection, anti-rabbit or anti-mouse immunoglobulin (Ig) (Amersham, Tokyo, Japan) was diluted 1:5000. Protein binding was detected using the ECL system (Amersham).

Transient expression of PARD3

The full-length human *PARD3* cDNA (clone ID: IOH62499) was obtained from Invitrogen (Carlsbad, CA, USA) and was subcloned into pcDNA3.2/V5-DEST vector (Invitrogen) to generate a mammalian expression vector. The *PARD3* expression vector, or an empty vector, was transfected into KYSE30 and KYSE270 cells using the Effectene Transfection Reagent Kit (Qiagen) according to the manufacturer's instructions. After 48 h incubation, the cell lysates were analysed by immunoblotting for detection of the expression of PAR-3 protein.

RNAi

Small interfering RNA duplex oligoribonucleotides targeting *PARD3* (5′-AAUGAUGGGUGUACGCAUGGCUUGG-3′) and control (non-silencing) siRNA duplexes were synthesized by Invitrogen in order to investigate the role of PAR-3 in ZO-1 localization and cell motility. The siRNAs were delivered into T.T cells using Lipofectamine RNAiMAX (Invitrogen), according to the manufacturer's protocol.

Immunofluorescence microscopy

KYSE30 and KYSE270 cells were transfected with the *PARD3* expression vector or the empty vector. T.T cells were transfected with either siRNA targeting *PARD3* or negative control siRNA. After 24 h incubation, the cells were collected, reseeded on glass slides and incubated overnight. The cells were fixed with 3.7% formaldehyde, permeabilized with 0.2% Triton X-100 and incubated with phosphate-buffered saline containing 1% bovine serum albumin. The cells were then treated with a mixture of anti-PAR-3 and anti-ZO-1 antibodies at a dilution of 1:500 and 1:100, respectively, for 1 h at 37 °C. The second antibodies used were a mixture of fluorescein isothiocyanate-conjugated anti-rabbit Ig (Cappel, Aurora, OH, USA) and rhodamine-conjugated anti-mouse Ig (Cappel) for the detection of PAR-3 and ZO-1, respectively. Samples were examined using a confocal laser scanning microscope (SV1000; Olympus, Tokyo, Japan).

Monolayer wound healing assay

T.T cells were transfected with either siRNA targeting *PARD3* or negative control siRNA, or left untreated. After 24 h, cells in Dulbecco's modified Eagle's medium with 1% fetal bovine serum were seeded on glass slides and allowed to adhere overnight. Wounds were scratched into the cell monolayer using a sterile 200-μl pipette tip, rinsed the cells with phosphate-buffered saline and added Dulbecco's modified Eagle's medium containing 10% fetal bovine serum with mitomycin C (0.5 μg/ml, Nacalai Tesque, Kyoto, Japan). Mitomycin C blocks mitosis and thus allows analysis of cell migration in the absence of cell proliferation. Cells were allowed to migrate into the wound over a period of 24 h before fixation. Wound widths were measured in three randomly selected regions at 0, 12 and 24 h after wounding. Cells were stained with Giemsa stain (Nacalai Tesque, Kyoto, Japan). Experiments were repeated at least three times.

Statistical analysis

Statistical analyses were carried out using SPSS 15.0 software (SPSS, Chicago, IL, USA). χ^2 or Wilcoxon signed-rank test was used. *P*-values of <0.05 were considered significant.

Conflict of interest

The authors declare no conflict

Acknowledgements

This study was supported by Grants-in-Aid for Scientific Research (18390223 and 20590408) from the Japan Society for the Program of Science (KY).

References

Aoki T, Mori T, Du X, Nisihira T, Matsubara T, Nakamura Y (1994). Allelotype study of esophageal carcinoma. *Genes Chromosomes Cancer* **10**: 177 182.

Assémat E, Bazellières E, Pallesi-Pocachard E, Le Bivic A, Massey-Harroche D. (2008). Polarity complex proteins. *Biochim Biophys Acta* **1778**: 614 630.

Berggren P, Kumar R, Sakano S, Hemminki L, Wada T, Steineck G *et al.* (2003). Detecting homozygous deletions in the CDKN2A (p16(INK4a))/ARF(p14(ARF)) gene in urinary bladder cancer using real-time quantitative PCR. *Clin Cancer Res* **9**: 235 242.

Chen X, Macara IG. (2005). Par-3 controls tight junction assembly through the Rac exchange factor Tiam1. *Nat Cell Biol* **7**: 262 269

Enzinger PC, Mayer RJ. (2003). Esophageal cancer. *N Engl J Med* **349**: 2241 2252.

Fang CM, Xu YH. (2001). Down-regulated expression of atypical PKC-binding domain deleted asip isoforms in human hepatocellular carcinomas. *Cell Res* **11**: 223 229.

Friend SH, Bernards R, Rogelj S, Weinberg RA, Rapaport JM, Albert DM *et al.* (1986). A human DNA segment with properties of the gene that predisposes to retinoblastoma and osteosarcoma. *Nature* **323**: 643 646.

Gao L, Macara IG, Joberty G. (2002). Multiple splice variants of Par3 and of a novel related gene, Par3L, produce proteins with different binding properties. *Gene* **294**: 99 107

Hahn SA, Schutte M, Hoque AT, Moskaluk CA, da Costa LT, Rozenblum E *et al.* (1996). DPC4, a candidate tumor suppressor gene at human chromosome 18q21.1. *Science* **271**: 350 353.

Hirose T, Karasawa M, Sugitani Y, Fujisawa M, Akimoto K, Ohno S *et al.* (2006). PAR3 is essential for cyst-mediated epicardial development by establishing apical cortical domains. *Development* **133**: 1389 1398.

Humbert PO, Dow LE, Russell SM. (2006). The Scribble and Par complexes in polarity and migration: friends or foes? *Trends Cell Biol* **16**: 622 630.

Inagaki Y, Yasui K, Endo M, Nakajima T, Zen K, Tsuji K *et al.* (2008). CREB3L4, INTS3, and SNAPAP are targets for the 1q21 amplicon frequently detected in hepatocellular carcinoma. *Cancer Genet Cytogenet* **180**: 30 36.

Izumi Y, Hirose T, Tamai Y, Hirai S, Nagashima Y, Fujimoto T *et al.* (1998). An atypical PKC directly associates and colocalizes at the epithelial tight junction with ASIP, a mammalian homologue of *Caenorhabditis elegans* polarity protein PAR-3. *J Cell Biol* **143**: 95 106.

Joberty G, Petersen C, Gao L, Macara IG. (2000). The cell-polarity protein Par6 links Par3 and atypical protein kinase C to Cdc42. *Nat Cell Biol* **2**: 531 539.

Kamb A, Gruis NA, Weaver-Feldhaus J, Liu Q, Harshman K, Tavtigian SV *et al.* (1994). A cell cycle regulator potentially involved in genesis of many tumor types. *Science* **264**: 436 440.

Kemphues KJ, Priess JR, Morton DG, Cheng NS. (1988). Identification of genes required for cytoplasmic localization in early *C. elegans* embryos. *Cell* **52**: 311 320.

Kennedy GC, Matsuzaki H, Dong S, Liu WM, Huang J, Liu G *et al.* (2003). Large-scale genotyping of complex DNA. *Nat Biotechnol* **21**: 1233 1237.

Kohjima M, Noda Y, Takeya R, Saito N, Takeuchi K, Sumimoto H. (2002). PAR3beta, a novel homologue of the cell polarity protein PAR3, localizes to tight junctions. *Biochem Biophys Res Commun* **299**: 641 646.

Li J, Yen C, Liaw D, Podsypanina K, Bose S, Wang SI *et al.* (1997). PTEN, a putative protein tyrosine phosphatase gene mutated in human brain, breast, and prostate cancer. *Science* **275**: 1943 1947.

Lin D, Edwards AS, Fawcett JP, Mbamalu G, Scott JD, Pawson T. (2000). A mammalian PAR-3 PAR-6 complex implicated in Cdc42/Rac1 and aPKC signalling and cell polarity. *Nat Cell Biol* **2**: 540 547

Macara IG. (2004). Parsing the polarity code. *Nat Rev Mol Cell Biol* **5**: 220 231.

Mei R, Galipeau PC, Prass C, Berno A, Ghandour G, Patil N *et al.* (2000). Genome-wide detection of allelic imbalance using human SNPs and high-density DNA arrays. *Genome Res* **10**: 1126 1137

Nagayama K, Kohno T, Sato M, Arai Y, Minna JD, Yokota J. (2007). Homozygous deletion scanning of the lung cancer genome at a 100-kb resolution. *Genes Chromosomes Cancer* **46**: 1000 1010.

Nannya Y, Sanada M, Nakazaki K, Hosoya N, Wang L, Hangaishi A *et al.* (2005). A robust algorithm for copy number detection using high-density oligonucleotide single nucleotide polymorphism genotyping arrays. *Cancer Res* **65**: 6071 6079.

Stevenson BR, Siliciano JD, Mooseker MS, Goodenough DA. (1986). Identification of ZO-1: a high molecular weight polypeptide associated with the tight junction (zonula occludens) in a variety of epithelia. *J Cell Biol* **103**: 755 766.

Suzuki A, Ohno S. (2006). The PAR aPKC system: lessons in polarity. *J Cell Sci* **119**: 979 987.

Vizcaino AP, Moreno V, Lambert R, Parkin DM. (2002). Time trends incidence of both major histologic types of esophageal carcinomas in selected countries, 1973 1995. *Int J Cancer* **99**: 860 868.

Wodarz A, Näthke I. (2007). Cell polarity in development and cancer. *Nat Cell Biol* **9**: 1016 1024.

Yasui K, Imoto I, Fukuda Y, Pimkhaokham A, Yang ZQ, Naruto T *et al.* (2001). Identification of target genes within an amplicon at 14q12 q13 in esophageal squamous cell carcinoma. *Genes Chromosomes Cancer* **32**: 112 118.

Zhao X, Li C, Paez JG, Chin K, Jänne PA, Chen TH *et al.* (2004). An integrated view of copy number and allelic alterations in the cancer genome using single nucleotide polymorphism arrays. *Cancer Res* **64**: 3060 3071.

Zitzelsberger H, Hieber L, Richter H, Unger K, Briscoe CV, Peddie C *et al.* (2004). Gene amplification of atypical PKC-binding PARD3 in radiation-transformed neoplastic retinal pigment epithelial cell lines. *Genes Chromosomes Cancer* **40**: 55 59.

Supplementary Information accompanies the paper on the Oncogene website (http://www.nature.com/onc)

Liver International ISSN 1478-3223

CLINICAL STUDIES

Oxidative stress may enhance the malignant potential of human hepatocellular carcinoma by telomerase activation

Taichiro Nishikawa, Tomoki Nakajima, Tatsuo Katagishi, Yoshihisa Okada, Masayasu Jo, Keizo Kagawa, Takeshi Okanoue, Yoshito Itoh and Toshikazu Yoshikawa

Kyoto Prefectural University of Medicine Graduate School of Medical Science, Molecular Gastroenterology and Hepatology, Kyoto, Japan

Keywords
Akt – 8-OHdG – HCC – hTERT – PTEN – telomere

Abbreviations
DAPI, 4-6-diamidino-2-phenylindole; 8-OhdG, 8-hydroxy-2′-deoxyguanosine; FITC, fluorescein isothiocyanate; HCC, human hepatocellular carcinoma; hTERT, human telomerase reverse transcriptase; OS, oxidative stress; PNA, peptide nucleic acid; PTEN, phosphatase and tensin homolog deleted on chromosome 10; ROS, reactive oxygen species; RTA, relative telomerase activity; TRAP, telomere repeat amplification protocol.

Correspondence
Taichiro Nishikawa, Kyoto Prefectural University of Medicine Graduate School of Medical Science, Molecular Gastroenterology and Hepatology, Kyoto, Japan
Tel: +81 75 251 5519
Fax: +81 75 251 0710
e-mail: liverresearch2004@yahoo.co.jp

Received 2 September 2008
Accepted 7 November 2008

DOI:10.1111/j.1478-3231.2008.01963.x

Abstract

Background/Aims: Continuous oxidative stress (OS) plays an important role in the progression of chronic liver diseases and hepatocarcinogenesis through telomere shortening in hepatocytes. However, it has not been established how the OS influences the progression of human hepatocellular carcinomas (HCCs). We examined the correlations of OS with telomere length of cancer cells, telomerase activity and other clinicopathological factors in 68 HCCs. *Methods:* The level of 8-hydroxy-2′-deoxyguanosine (8-OHdG) as a marker of OS was examined immunohistochemically and OS was scored in four grades (0–3). The telomere length of cancer cells was measured by quantitative fluorescence *in situ* hybridization. Telomerase activity was measured by (i) immunodetection of human telomerase reverse transcriptase (hTERT) and (ii) telomere repeat amplification protocol (TRAP) assay. Telomerase related proteins, phosphatase and tensin homolog deleted on chromosome 10 (PTEN) and Akt, and other clinicopathological factors were also evaluated. *Results:* As the OS grade increased, the average telomere length became significantly shorter in HCCs, especially in the hTERT-negative group. In the state of high-grade OS, hTERT-positive HCC cells showed more proliferative and less apoptotic features compared with hTERT-negative HCC cells. Telomerase activity, as measured by the TRAP assay, was strongly correlated with OS grade in HCCs. Furthermore, a high OS grade was correlated with the downexpression of PTEN and the activation of Akt. *Conclusions:* Oxidative stress enhanced the malignant potential of HCCs through the activation of telomerase, which raises the possibility of using OS as a marker for assessing the clinical state of HCCs.

Continuous oxidative stress (OS), which results from the generation of reactive oxygen species (ROS) by environmental factors or cellular mitochondrial dysfunction, has recently been associated with the progression of chronic liver diseases and hepatocarcinogenesis (1–3). Repeated necrosis and regeneration of hepatocytes induced by OS appear to accelerate the senescence of hepatocytes, giving them the appearance of cancer cells. These processes may be due to the shortening of the telomeres of hepatocytes.

Telomeres, hexameric DNA repeats $(TTAGGG)_n$ at the ends of chromosomes (4), increase chromosomal stability by preventing chromosomal rearrangements and end-to-end fusions. In normal somatic cells, telomere shortening occurs during each cell division (5) and eventually leads to cell cycle arrest and apoptosis (6). In cancer cells, the length of telomeres is maintained by the expression of telomerase, which endows cancer cells with immortality and an ability to proliferate without any limit.

OS accelerates the shortening of the telomeres of human cells by inducing oxidative single-stranded damage in telomeric DNA (7, 8). Fibrosis and cirrhosis in liver have been attributed to OS-induced telomere shortening (9, 10). In hepatocytes, telomere shortening can be carcinogenic because it can lead to genetic changes such as telomerase activation (11). Whereas OS has such effects on normal liver cells, it is unclear whether it also has a role in the progression of hepatic cancer cells, especially with respect to telomeres and telomerase.

In this study, we investigated the effects of OS in human hepatocellular carcinomas (HCCs). Our findings indicate that OS promotes the development of HCCs and increases

their resistance to treatment and is associated with shortened telomeres and increased telomerase activity.

Materials and methods

Tissue preparation and patients

All HCC specimens were obtained from 63 patients who underwent partial hepatectomy and five patients who underwent needle biopsy in 1992–2005 in Kyoto Prefectural University of Medicine. None of the specimens had undergone any treatments such as percutaneous ethanol injection therapy or transcatheter arterial embolization before the collections. The clinicopathological parameters of these patients and the clinicopathological status of their HCC samples are shown in Table 1. Fourteen patients were positive for serum hepatitis B surface antigen, 45 were positive for anti-hepatitis C antibody, one was positive for both and eight were negative for both. Of the 68 patients, two had normal livers, 29 had chronic hepatitis and 37 had liver cirrhosis. Specimens were fixed in 4% buffered paraformaldehyde for 12–24 h, embedded in paraffin and cut into 5-μm-thick sections for use as described below. All 68 HCC paraffin blocks included non-cancerous tissues, which served as controls. Additionally, parts of 30 specimens were stored at −80 °C for later use in the telomere repeat amplification protocol (TRAP) assay (described below). Sixty-eight HCC specimens were stained with haematoxylin and eosin and classified according to their differentiation status according to the criteria of the Liver Cancer Study Group of Japan. Of these specimens, 29 were classified as well differentiated, 28 were classified as moderately differentiated and 11 were classified as poorly differentiated. The degree of necroinflammatory activity and fibrosis of non-cancerous tissues were classified according to the international classification (12) by haematoxylin and eosin and Masson trichrome staining. Informed consent to our using HCC specimens for this study was obtained from all patients according to the guidelines approved by our hospital ethical committee.

Table 1. Age and sex of 68 human hepatocellular carcinoma patients and the clinicopathological status of their human hepatocellular carcinoma samples

Sex	
Male	43
Female	25
Age (years) (mean ± SD)	
Range	25–77
Mean ± SD	62.6 ± 8.15
Aetiology	
HBV	14
HCV	45
HBV+HCV	1
Non-HBV, non-HCV	8
Non-cancerous tissue	
Normal liver	2
Chronic hepatitis	29
Liver cirrhosis	37
Tumour size (mm)	12–160
Tumour stage	
I	10
II	46
III	9
IV	3
Tumour differentiation	
Well differentiated	29
Moderately differentiated	28
Poorly differentiated	11

HBV, hepatitis B virus; HCV, hepatitis C virus; SD, standard deviation.

Immunohistochemical analysis

Sections were deparaffinized, immersed in 0.3% H_2O_2–methanol for 20 min, autoclaved at 120 °C for 20 min in a Target Retrieval Solution (DakoCytomation, Kyoto, Japan), incubated in blocking buffer (Tris buffered saline containing 2% fetal bovine serum) to block non-specific reactions and incubated with one of the four primary antibodies diluted 1:100 in the blocking buffer at 4 °C overnight. The antibodies were mouse anti-Ki-67 monoclonal antibody (DakoCytomation), rabbit anti-phosphatase and tensin homolog deleted on chromosome 10 (PTEN) monoclonal antibody (Cell Signaling Technology Inc., Beverly, MA, USA) and rabbit anti-phospho-AKT (Ser473) monoclonal antibody (Cell Signaling Technology Inc.). The remaining procedure was based on the standard streptavidin–biotin–peroxidase complex method (13). Positive reactions were visualized using diaminobenzidine (DAB; Wako, Osaka, Japan) as a substrate. The sections were counterstained with haematoxylin. Each immunohistochemical analysis included a slide without the primary antibody as a negative control. The Ki-67 index, an indicator of tumoral proliferative activity, was defined as the number of Ki-67 antibody-positive cells per 1000 scored cancer cells.

8-Hydroxy-2′-deoxyguanosine immunohistochemistry

Following the method of Kato *et al.* (13), 1000–2000 cancer or normal hepatic cells from HCC or non-cancerous tissues were stained with antibody against 8-hydroxy-2′-deoxyguanosine (8-OhdG), a marker of oxidative DNA damage. Immunoreactive cells were detected as described above and were counted by two hepatologists (T. N. and T. N.). The degree of OS was classified according to the percentage of 8-OhdG-positive cells: Grade 0, < 10%; Grade 1, 10–50%; Grade 2, 50–90%; Grade 3, > 90%.

Human telomerase reverse transcriptase immunohistochemistry

Human telomerase reverse transcriptase (hTERT), a telomerase catalytic subunit, is an indicator of telomerase activity in cancer cells (14). hTERT was immunohistochemically detected with mouse anti-hTERT monoclonal antibody (Novocastra, Newcastle Upon Tyne, UK) as

described above. Lymphocytes, in which hTERT is normally strongly expressed (15), were used as a positive control.

Transferase-mediated deoxy uridine triphosphate nick end labelling

Apoptosis in HCC tissues was assessed using the transferase-mediated deoxy uridine triphosphate nick end-labelling technique (16). The signals were visualized with DAB and counterstained with haematoxylin. The apoptosis index was defined as the number of immunoreactive cells per 1000 scored cancer cells.

Telomere repeat amplification protocol assay

Telomerase activity was also semiquantitatively measured by a TRAP assay using a TRAPEZE Telomerase Detection Kit (Oncor, Gaithersburg, CA, USA) according to the manufacturer's protocol. Thirty frozen HCC samples were examined as described in supplementary method 1. Relative telomerase activities (RTAs) were classified into four groups: 0 (RTA was not detectable), 1+ ($0 < RTA < 50$), 2+ ($50 \leqq RTA < 100$) and 3+ ($100 \leqq RTA$).

Analysis of telomere length by quantitative fluorescence *in situ* hybridization

Telomeres were identified in the paraffin sections using a telomere-specific peptide nucleic acid fluorescence *in situ* hybridization kit as described previously (17). The sections were counterstained with 4′-6-diamidino-2-phenylindole (DAPI) (1000 ng/ml, VYS-32-804830, ABBOTT JAPAN CO., Tokyo, Japan). Following the protocol of Meeker *et al.* (18), image-processed telomeric signals were quantified from digitized fluorescence microscopic images using the image analysis software package IP LABS (version 3.54, Scanalytics, Fairfax, VA, USA). Lymphocytes were used as internal controls of the telomeric signal because the telomere lengths of the lymphocytes were less affected by ageing than those of somatic cells (19). The telomeric pixel intensities of 15–20 nuclei of cancer cells and 5–10 nuclei of lymphocytes were recorded. To correct the different amounts of DNA in the sectioned nuclei, the telomeric signal intensity was modified by dividing the pixel intensity of the telomere signal for a given nucleus by the pixel intensity of the DAPI signal within that nucleus, as reported previously (18). Average telomere length was defined as Tel-T/Tel-L, where Tel-T and Tel-L are the average modified telomeric signal intensities of cancer cells and lymphocytes, respectively, measured in four different fields per sample.

Statistical analysis

The data are represented as the mean and SD in each category. The correlations of OS grade in HCC tissues to different clinicopathological and biochemical factors were assessed using the Kruskal–Wallis H test, the Spearman's Rank Correlation Coefficient and the Mann–Whitney U test. Differences of clinicopathological factors between hTERT-negative and hTERT-positive HCCs were analysed using the Mann–Whitney U test. $P < 0.05$ was considered to be statistically significant. All the tests were analysed using the STATVIEW program (Abacus Concepts, Berkeley, CA, USA).

Results

Immunohistochemical analysis of 8-hydroxy-2′-deoxyguanosine in human hepatocellular carcinoma samples

HCC tissues representative of each OS grade are shown in Figure 1a. 8-OHdG was mainly found in the nuclei of cancer cells, but it was also found in the nuclei of lymphocytes and fibroblasts and hepatocytes in non-cancerous tissues. The OS grades of the HCC tissues were: 15 Grade 0, 17 Grade 1, 15 Grade 2 and 21 Grade 3. None of several clinicopathological parameters of the 68 subjects (age, sex, etc.) was significantly related to the OS grade (Table 2). Furthermore, no tumour factors (differentiation of HCC tissues, size, stage or etiology) was significantly related to the OS grade (Table 3). On the other hand, the OS grade of non-cancerous tissues was significantly related to the patient's age, etiology and grading of chronic hepatitis ($P < 0.05$, Kruskal–Wallis H test and Spearman's rank correlation coefficient, Table 4).

Immunohistochemical analysis of human telomerase reverse transcriptase in human hepatocellular carcinoma samples

hTERT, an indicator of telomerase activity in cancer cells (14), was immunodetected in lymphocytes, in which it is normally expressed (15) (Fig. 1b, left panel), and in some cancer cells, but not in other cells, including normal hepatocytes. hTERT in HCC cells was mainly localized in the nucleus, especially in the nucleolus (Fig. 1b, right panel). It was also weakly detected in the cytoplasm of HCCs (Fig. 1b, left panel). Of the 68 HCC specimens examined, 47 were judged hTERT-positive (strong detection) and 21 were judged hTERT-negative (no or weak detection) (Table 3).

Oxidative stress shortens telomere length in human hepatocellular carcinoma samples

The telomere signals of cancer cells and lymphocytes were detected as green fluorescein isothiocyanate signals within the blue DAPI signals (the nuclear signals of cancer cells and lymphocytes) (Fig. 1c). Extensive OS was found to significantly accelerate the shortening of telomeres in cancer cells ($P < 0.001$, Kruskal–Wallis H test, Table 3). As the OS grade increased, the average telomere length of cancer cells strongly decreased in hTERT-negative HCCs ($P < 0.001$) whereas it did not

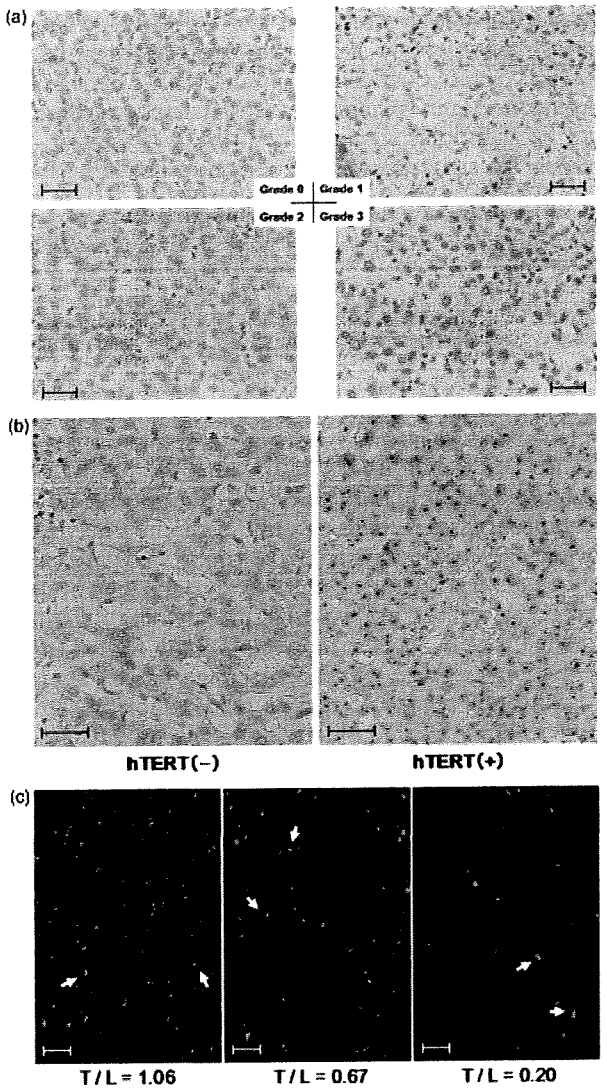

Fig. 1. Representative photographs of immunostaining and quantitative fluorescence *in situ* hybridization of human hepatocellular carcinoma (HCC) tissues. (a) Immunostaining of 8-hydroxy-2′-deoxyguanosine. The staining intensity was classified into four grades according to the percentage of immunoreactive cells. (b) Immunostaining of human telomerase reverse transcriptase (hTERT). In hTERT-negative HCCs, the cytoplasm of the cancer cell was faintly stained and the lymphocytes were strongly stained. In hTERT-positive HCCs, the nucleus, especially the nucleolus of the cancer cells, was strongly stained. (c) Representative photographs of quantitative fluorescence *in situ* hybridization for measurement of telomere length. White and red arrows in each photograph indicate the lymphocytes and the cancer cells in HCC tissues respectively. T/L below each photograph represents the average value of the mean Tel-T/mean Tel-L as the average telomere length of cancer cells in each HCC tissue, where mean Tel-T and mean Tel-L represent the average modified telomeric signal intensity of cancer cells and lymphocytes respectively. Scale bars, 50 μm.

significantly change in hTERT-positive HCCs (Fig. 2a). The difference between the average telomere lengths in hTERT-positive and hTERT-negative HCCs significantly increased with increasing OS grade ($P < 0.05$, Mann–Whitney U test, Fig. 2b).

Oxidative stress increases telomerase activity in human hepatocellular carcinoma samples

The immunodetection of hTERT in HCC tissues was significantly correlated with OS grade ($P < 0.001$, Kruskal–Wallis H test, Fig. 2b). Additionally, samples with higher OS grades had higher RTA scores in the TRAP assay ($P < 0.05$, Spearman's rank correlation coefficient, Fig. 2c). The degree of tumour differentiation was significantly related to hTERT expression in HCC tissues but was not related to the length of telomeres (Table 5).

Increased proliferative activity and apoptotic resistance in human hepatocellular carcinoma samples by oxidative stress through telomerase activation

We did not observe a correlation between the Ki-67 index, an indicator of tumoral proliferative activity, and OS grade in HCC tissues (Table 3), although we could not rule out the possibility that the Ki-67 index had a weak positive correlation with the OS grade in the hTERT-positive group and a weak negative correlation with the OS grade in the hTERT-negative group (Fig. 2d). On the other hand, OS was significantly correlated with the apoptosis index in HCC tissues ($P < 0.05$, Kruskal–Wallis H test, Table 3), especially in the hTERT-negative group ($P < 0.001$) (Fig. 2e). For OS Grades 2 and 3, the hTERT-positive HCC cells showed a significantly higher proliferative activity and a significantly higher apoptotic resistance than the hTERT-negative HCC cells ($P < 0.05$, Mann–Whitney U test, Fig. 2f). Additionally, malignancy parameters of HCC tissues (Ki-67 index, apoptosis index, differentiation and stage) were not significantly different between the OS Grades 0–1 and 2–3 groups in HCC tissues (Table 6). However, the Ki-67 index and differentiation were significantly different between the OS Grade 0–1 group and the OS Grade 2–3 and hTERT-positive group in HCC tissues ($P < 0.05$, Mann–Whitney U test, Table 6).

Downexpression of phosphatase and tensin homolog deleted on chromosome 10 and activated phosphorylation of AKT in human hepatocellular carcinoma samples by oxidative stress

Phospho-AKT (P-AKT), a regulator of telomerase activity (20, 21), was detected in the nucleus and the cytoplasm of cancer cells (Fig. 3a, panel A). PTEN, an inhibitor of Akt phosphorylation (22), was not detected in the same lesions (panel B). On the other hand, PTEN was detected strongly in the cytoplasm and weakly in the nucleus in cancer cells that were P-AKT negative (panels C and D). Staining of PTEN was stronger in the non-cancerous part of an HCC sample (N in panel E) than in the cancerous part (T), as reported previously (23). As

Table 2. The correlation between the oxidative stress grades of 68 human hepatocellular carcinoma samples and the clinicopathological parameters of their human hepatocellular carcinoma patients

	8-OHdG				
	Grade 0 ($n=15$)	Grade 1 ($n=17$)	Grade 2 ($n=15$)	Grade 3 ($n=21$)	*P*-value
Sex (M/F)	11/4	11/7	10/6	11/10	0.5808
Age (years)	61.9 ± 8.4	64.1 ± 6.3	59.3 ± 13.0	63.6 ± 6.3	0.6465
BMI (kg/m^2)	22.9 ± 3.6	23.7 ± 2.7	21.9 ± 3.2	24.0 ± 2.3	0.3415
AST (IU/L)	63.4 ± 35.1	62.9 ± 43.5	62.5 ± 42.9	45.5 ± 22.7	0.5273
ALT (IU/L)	70.3 ± 39.8	53.6 ± 29.0	58.3 ± 42.1	40.8 ± 23.0	0.1700
PLT (× 10^4/μl)	13.6 ± 6.3	12.8 ± 4.8	13.4 ± 6.3	12.9 ± 7 1	0.9507
ALB (g/dl)	3.85 ± 0.49	4.20 ± 0.47	4.15 ± 0.28	4.15 ± 0.43	0.2689
ICG15 (%)	22.8 ± 13.5	13.9 ± 8.1	17.5 ± 12.1	14.6 ± 12.1	0.2684
AFP (μg/ml)	5860 ± 19 708	7458 ± 2215	294 ± 897	11 936 ± 46 136	0.7615
PIVKA-II (mAU/ml)	1211 ± 4372	1936 ± 5316	334 ± 510	394 ± 1113	0.9807

Data are expressed as mean ± SD.

Statistical analysis was performed using the Kruskal–Wallis *H*-test.

ALB, albumin; ALT, alanine aminotransferase; AFP, á-foetoprotein , AST, aspartate aminotransferase; BMI, body mass index; 8-OHdG, 8-hydroxy-2′-deoxyguanosine; F, female; ICG, indocyanine green; M, male; PLT, platelet; SD, standard deviation.

Table 3. Correlations between the oxidative stress grades of 68 human hepatocellular carcinoma samples and clinicopathological factors

	8-OHdG				
	Grade 0 ($n=15$)	Grade 1 ($n=17$)	Grade 2 ($n=15$)	Grade 3 ($n=21$)	*P*-value
T-length (T/L)	1.097 ± 0.198	0.599 ± 0.271	0.549 ± 0.209	0.822 ± 0.663	0.00008110**
hTERT (N/P)	15/0	15/2	10/5	7/14	0.00006758**
Telomerase (0/1/2/3)	2/3/0/0	1/4/1/0	2/2/3/1	0/4/5/2	0.002539*
Ki-67 index	13.41 ± 8.43	13.41 ± 7 14	14.74 ± 9.87	15.75 ± 9.09	0.8654
Apo index	1.218 ± 0.720	1.782 ± 0.913	2.526 ± 1.372	2.306 ± 1.976	0.04040*
Different (W/M/P)	9/5/1	7/8/2	7/5/3	6/10/5	0.05515
Size (mm)	44.53 ± 43.00	49.47 ± 37.81	45.86 ± 36.17	41.95 ± 20.12	0.5474
Stage (I/II/III/IV)	5/7/3/0	4/5/7/1	1/11/3/0	3/14/2/2	0.6141
Aetiology (B/C/B+C/NBNC)	3/9/1/2	2/13/0/2	5/9/0/1	4/14/0/3	0.5311
Non-tumour (N/CH/LC)	1/5/9	0/9/8	1/5/9	0/12/9	0.2674

Data are expressed as mean ± SD.

Statistical analysis was performed using the Spearman's rank correlation coefficient in telomerase, differentiation, stage and non-tumour and using the Kruskal–Wallis *H*-test in other factors.

*$P < 0.05$.

**$P < 0.001$.

Apo index, apoptosis index; B/C/B+C/NBNC, HBV/HCV/HBV+HCV/non-HBV, non-HCV; Different, tumour differentiation; 8-OHdG, 8-hydroxy-2′-deoxyguanosine; HBV, hepatitis B virus; HCV, hepatitis C virus; hTERT, human telomerase reverse transcriptase; N/P, negative/positive; NL/CH/LC, normal liver/chronic hepatitis/liver cirrhosis; SD, standard deviation; T-length, telomere length; T/L, tumour cell/lymphocyte; W/M/P, well differentiated/moderately differentiated/poorly differentiated.

the OS grade increased, the level of Akt phosphorylation in HCC samples increased significantly ($P < 0.001$, Fig. 3b) and the expression of PTEN in HCC samples decreased significantly ($P < 0.05$, Fig. 3b). These results suggest that the activation of telomerase by OS in HCC tissues is due to the downexpression of PTEN and the following activation of Akt.

Discussion

Although OS has been associated with chronic liver disease (24, 25), whether it has a role in the clinicopathology of HCC has not been investigated previously. In the present study, most HCC tissues (53/68, 77.9%) had high levels of OS (OS grades over 1). However, the 8-OHdG levels in the cancerous parts were not significantly related to those in the non-cancerous parts (Table 4). This suggests that the cause of OS in HCC cells is different from that in hepatocytes in chronic liver diseases.

Furthermore, the OS grade in HCC tissues was not significantly correlated with several clinicopathological factors of HCC samples, such as degree of differentiation, size, stage, etiology and type of non-cancerous tissue

Table 4. The correlation between the oxidative stress grades of 68 non-cancerous tissues and the clinicopathological parameters of their patients

	8-OHdG				
	Grade 0 ($n=14$)	Grade 1 ($n=22$)	Grade 2 ($n=19$)	Grade 3 ($n=13$)	*P*-value
Sex (M/F)	9/5	13/9	10/9	10/3	0.6944
Age (years)	60.0 ± 6.4	60.2 ± 9.4	66.1 ± 7.0	64.2 ± 7.2	0.04901*
BMI (kg/m^2)	23.5 ± 2.1	21.9 ± 2.8	23.9 ± 2.7	24.1 ± 2.7	0.1493
AST (IU/L)	61.0 ± 46.0	58.2 ± 36.3	57 1 ± 36.3	66.0 ± 33.6	0.7817
ALT (IU/L)	60.5 ± 38.5	53.0 ± 29.8	54.6 ± 40.1	65.4 ± 37.8	0.7232
PLT (× 10^4/μl)	13.9 ± 8.5	12.4 ± 5.8	14.8 ± 4.9	12.0 ± 5.4	0.2568
ALB (g/dl)	4.12 ± 0.28	4.11 ± 0.55	4.05 ± 0.45	4.18 ± 0.32	0.7337
ICG15 (%)	22.8 ± 13.5	13.9 ± 8.1	17.5 ± 12.1	14.6 ± 12.1	0.2684
Aetiology (B/C/B+C/NBNC)	5/9/0/0	8/12/2/0	1/14/3/1	0/11/2/0	0.01378*
Grading (A0/A1/A2/A3)	0/11/2/1	0/12/9/1	1/8/9/1	1/2/5/5	0.003754*
Staging (F0/F1/F2/F3/F4)	0/2/4/0/8	0/2/4/6/10	1/1/5/3/9	1/0/0/3/9	0.1893
OS tumour (G0/G1/G2/G3)	4/2/3/5	6/8/2/6	4/5/4/6	1/2/6/4	0.1679

Data are expressed as mean ± SD.

Statistical analysis was performed using the Spearman's rank correlation coefficient in grading, staging and OS tumour and using the Kruskal–Wallis *H*-test in other factors.

*$P < 0.05$.

ALB, albumin; ALT, alanine aminotransferase; AST, aspartate aminotransferase; B/C/B+C/NBNC, HBV/HCV/HBV+HCV/non-HBV, non-HCV; BMI, body mass index; 8-OHdG, 8-hydroxy-2′-deoxyguanosine; HBV, hepatitis B virus; HCC, human hepatocellular carcinoma; HCV, hepatitis C virus; ICG, indocyanine green; OS, oxidative stress; OS tumour, 8-OHdG grade of HCC tissue; PLT, platelet; SD, standard deviation.

(Table 3), although the OS grade in non-cancerous tissues was significantly correlated with several clinicopathological factors (Table 4). Tumour cells produce ROS at a far greater rate than do non-tumour cells *in vitro* and *in vivo* (26, 27). The increased ROS in HCC tissues may be due to hypoxia (28), which arises from the high proliferative activity and high cellular density of cancer cells. OS is also a mediator of angiogenesis signalling (29), which suggests that one of the effects of OS is to counteract the effects of hypoxia.

Our findings that OS in HCC tissues significantly accelerated telomere shortening and increased the apoptosis of cancer cells (Table 3) are consistent with our previous reports that OS hastened the telomere shortening of hepatocytes in chronic hepatitis C and non-alcoholic fatty liver disease (30, 31). Thus, OS appears to promote the senescence of cancer cells in HCC tissues through telomere shortening, as it does in hepatocytes in chronic liver diseases. OS also inhibits the proliferation of normal hepatocytes through telomere shortening (30). However, OS was not associated with the proliferative activity of HCC cells in this study, including hTERT-negative HCCs (Fig. 2d). Cancer cells with a high proliferative activity appear to be in a hypermetabolic state and appear to generate much cellular ROS. Additionally, the cell cycle checkpoint usually breaks down during carcinogenesis. Therefore, HCCs with high levels of OS may proliferate despite the OS-induced telomere shortening.

As the OS grade increased, the immunodetection of hTERT and telomerase activity in HCC tissues increased (Table 3). Although hTERT mRNAs were detected in the hepatocytes and in the serum of patients with chronic liver disease (32, 33), we were unable to detect hTERT protein in non-cancerous parts including liver tissues from patients with chronic hepatitis or liver cirrhosis. These results suggest that hTERT is immunodetected much more strongly in HCC tissues than in non-cancerous tissues. In agreement with previous reports (34, 35), HCC cells in the hTERT-positive group tended to have a higher proliferative activity and higher apoptotic resistance than did those in the hTERT-negative group, particularly in a highly oxidative-stressed environment (Fig. 2f). Additionally, HCC tissues with a high OS grade (2–3) and a high immunodetection of hTERT were significantly more proliferative and dedifferentiated than those with a low OS grade (0–1) (Table 6). Thus, OS in HCC tissues may increase the malignant potential of cancer cells by upregulating hTERT.

Although there is evidence that OS contributes to telomerase activation in HCC (36), the mechanism is unknown. In this study, we regarded the immunodetection of hTERT in the nucleus of cancer cells as an indicator of activated telomerase because the nuclear localization of hTERT is required to promote the elongation of telomere sequences within the cellular nucleus. hTERT must be phosphorylated before it can be translocated from the cytoplasm to the nucleus (37). Protein kinase B/Akt is known to be involved in the phosphorylation and the expression of hTERT (20, 21). Our finding that Akt is activated in HCC tissues with high-grade OS (Fig. 3b) is consistent with a report that OS increased the phosphorylation of Akt in human hepatoma cells *in vitro* (38). Additionally, the expression

of PTEN, a tumour suppressor and an inhibitor of the phosphorylation of Akt (22), significantly decreased in HCC tissues with increasing OS grade (Fig. 3b). OS may induce the inactivation of PTEN and the following activation of AKT in cancer cells (39). The downregulation and functional inactivation of PTEN may be a major mechanism of Akt phosphorylation by OS. Therefore, we assume that the PTEN–Akt pathway is a key factor in the activation of telomerase by OS in HCC tissues.

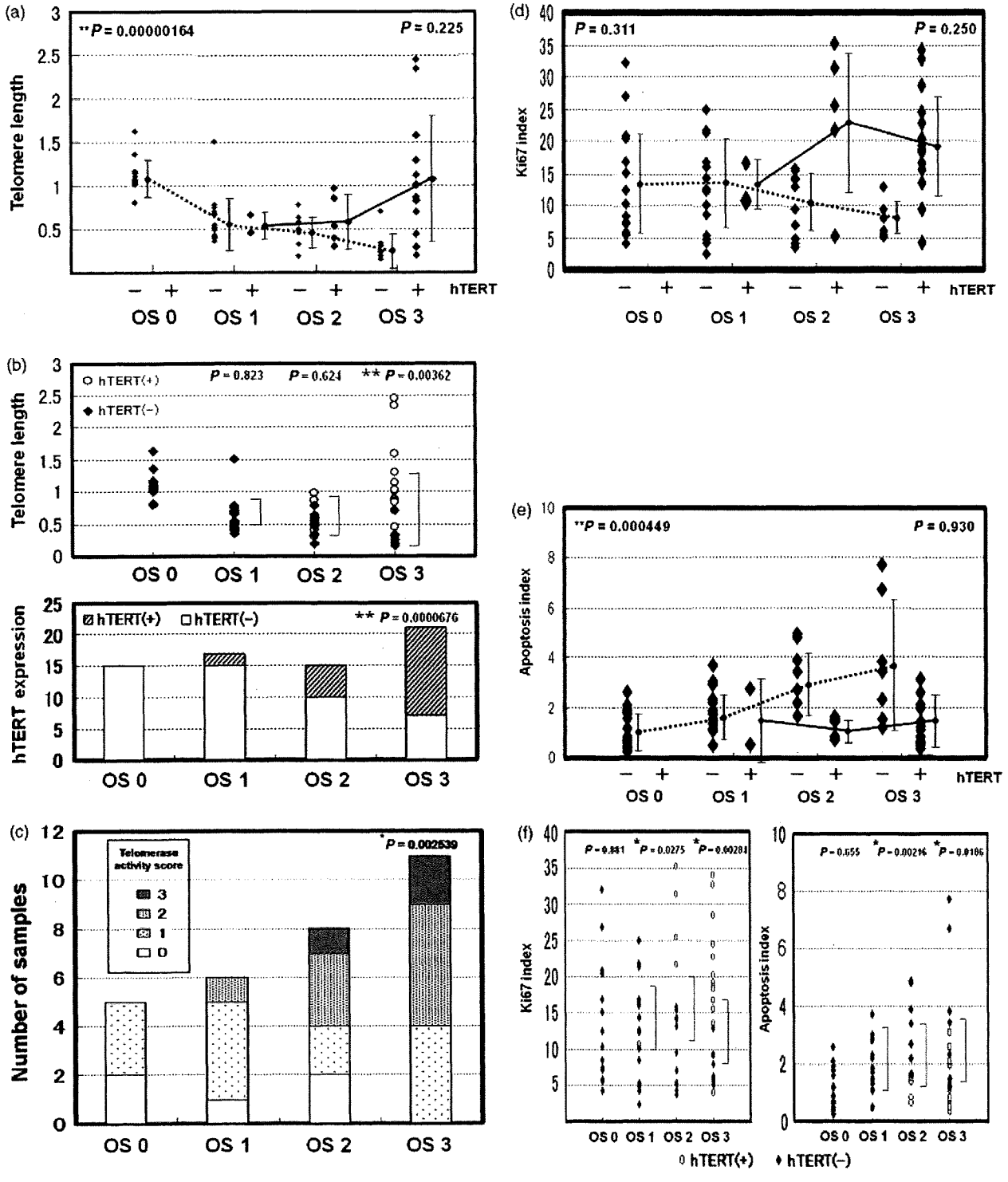

Liver International (2009)

Table 5. Human telomerase reverse transcriptase expression but not telomere length is related to the degree of tumour differentiation in 68 human hepatocellular carcinoma samples

	Histological grade of carcinoma			
Measurement	Well differentiated ($n = 15$)	Moderately differentiated ($n = 17$)	Poorly differentiated ($n = 15$)	*P*-value†
Telomere length‡	0.713 ± 0.329	0.835 ± 0.490	0.734 ± 0.653	0.4612
hTERT (N/P)§	24/5	18/10	5/6	0.01847*

†Statistical analysis was performed using the Kruskal–Wallis *H*-test.
‡Defined as T/L, where T and L are the telomere signal intensities of tumour cells and lymphocytes respectively. Data are expressed as mean ± SD.
§N/P, expression of hTERT in HCC tissues is negative/positive.
*$P < 0.05$.
HCC, human hepatocellular carcinoma; hTERT, human telomerase reverse transcriptase; SD, standard deviation.

Table 6. Correlations among the oxidative stress grade of human hepatocellular carcinomas, expression of human telomerase reverse transcriptase and clinicopathological factors

		Grades 2–3			
Measurement	Grades 0–1 ($n = 32$)	hTERT (−) ($n = 13$)	*P*-value	hTERT (+) ($n = 19$)	*P*-value
Ki-67 index	13.41 ± 7.65	15.33 ± 9.30	0.5349	20.57 ± 9.30	0.009035*
Apo index	3.591 ± 6.712	2.389 ± 1.695	0.2031	1.425 ± 0.886	0.3258
Differentiation (W/M/P)	16/13/1	13/15/8	0.05286	3/9/2	0.03283*
Stage (I/II/III/IV)	9/12/10/1	4/25/3/2	0.8865	0/14/3/2	0.3194

Data are expressed as mean ± SD.
Statistical analysis was performed using the Mann–Whitney *U*-test.
*$P < 0.05$.
Apo index, apoptosis index; differentiation, tumour differentiation; hTERT, human telomerase reverse transcriptase; W/M/P, well differentiated/moderately differentiated/poorly differentiated.

Our findings suggest that OS is associated with the malignant potential of HCCs through the activation of telomerase. Several drugs that are antioxidants are reported to prevent hepatocarcinogenesis and inhibit the growth of HCC cells (40, 41). We also recently demonstrated that epigallocatechin-3-gallate, a major polyphenol of green tea and a potent antioxidant, suppressed the growth of HCC cells *in vitro* and *in vivo* (42). These results raise the possibility of using antioxidant therapy to reduce OS in HCCs with high telomerase activity in order to inhibit the growth of HCCs. This is supported by the findings that the anticancer effects of antioxidants partially result from the downregulation of telomerase activity (43) and that inhibition of telomerase enhances the effects of chemotherapeutic agents in various cancer cells (44).

In conclusion, our findings show that HCC tissues are frequently characterized by OS, which contributes to the acceleration of telomere shortening and the activation of telomerase in cancer cells. The activation of telomerase by OS possibly results from the downexpression of PTEN and the phosphorylation of Akt. Because HCC cells that have high levels of hTERT as a result of OS are more malignant, continuous OS during the progression of HCCs may indicate a poor prognosis. Our results suggest that OS in HCC tissues can be used as a measure of the malignant potential.

Fig. 2. Oxidative stress (OS) accelerated telomere shortening, increased telomerase activity in human hepatocellular carcinoma (HCC) cells and was related to the increased proliferative activity and apoptotic resistance in HCC tissues through telomerase activation. (a) In human telomerase reverse transcriptase (hTERT)-negative HCCs, the average telomere length significantly decreased with increasing OS grade (dotted line) and in hTERT-positive HCCs, it elongated (solid line) (*$P < 0.05$, **$P < 0.001$ by the Kruskal–Wallis *H* test). (b) The average telomere length in hTERT-positive HCCs was elongated compared with those in hTERT-negative HCCs as the OS grade increased (upper) (by the Mann–Whitney *U* test). There was a positive correlation statistically between the OS grade and the expression of hTERT in HCC tissues (lower) (**$P < 0.001$ by the Kruskal–Wallis *H* test). (c) Distribution of telomerase activity among 30 HCC samples. Higher telomerase activity scores were more frequently observed in samples with higher OS grades (*$P < 0.05$ by Spearman's rank correlation coefficient). (d) The Ki-67 index in hTERT-negative HCCs (dotted line) and hTERT-positive HCCs (solid line) were not significantly affected by the OS grade (Kruskal–Wallis *H* test). (e) As the OS grade increased, the apoptosis index increased significantly in hTERT-negative HCCs (dotted line) but did not significantly change in hTERT-positive HCCs (solid line) (*$P < 0.05$, **$P < 0.001$ by the Kruskal–Wallis *H* test). (f) The Ki-67 index increased and the apoptosis index decreased in hTERT-positive HCCs compared with those in hTERT-negative HCCs, as the OS grade increased (*$P < 0.05$ by the Mann–Whitney *U* test). The data in (a), (d) and (e) show the mean and SD.

(a)

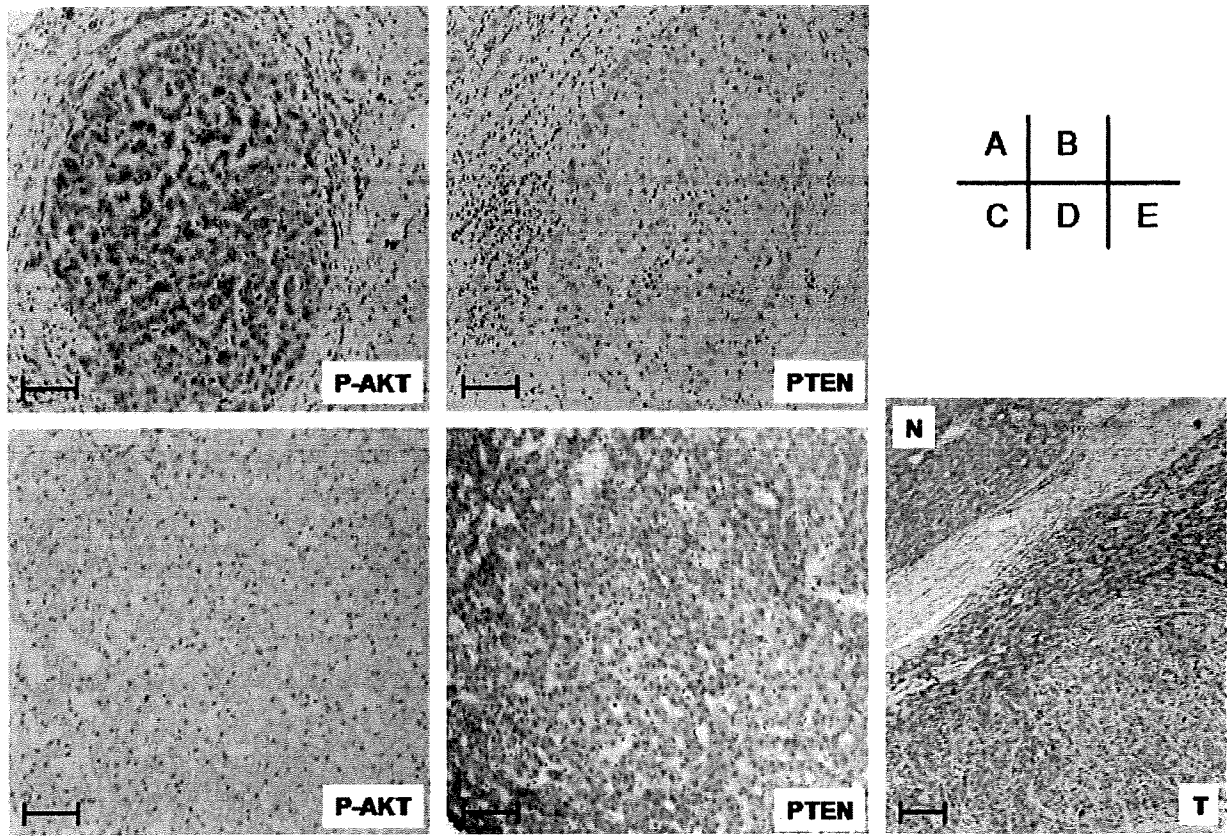

(b)

OS grade	P-AKT		PTEN	
	(–)	(+)	(–)	(+)
0 (*n*=15)	14	1	3	12
1 (*n*=17)	13	4	4	13
2 (*n*=15)	10	5	8	7
3 (*n*=21)	6	15	15	6
P-value	0.00013**		0.00435*	

Fig. 3. Oxidative stress (OS) increased the level of Akt phosphorylation and decreased the expression of phosphatase and tensin homolog deleted on chromosome 10 (PTEN) in human hepatocellular carcinoma (HCC) samples. (a) Representative photographs of immunostainings of phospho-Akt (P-AKT) in Ser473 and PTEN. P-AKT was detected in the nucleus and in the cytoplasm of cancer cells in the P-AKT-positive sample (A) and PTEN was not detected in the same lesion (B). Panel C shows a P-AKT-negative sample and PTEN was detected mainly in the cytoplasm of the cancer cells in the same lesion (D). Staining of PTEN was stronger in the non-cancerous part (N) than in the cancerous part (T) of the HCC sample (E). Scale bars, 50 μm. (b) The phosphorylation of Akt in HCC tissues significantly increased and the expression of PTEN in HCC tissues significantly decreased as the OS grade increased (*$P < 0.05$, **$P < 0.001$ by the Kruskal–Wallis *H* test).

Liver International (2009)

References

1. Jain SK, Pemberton PW, Smith A, *et al.* Oxidative stress in chronic hepatitis C: not just a feature of late stage disease. *J Hepatol* 2002; **36**: 805–11.
2. Aboutwerat A, Pemberton PW, Smith A, *et al.* Oxidant stress is a significant feature of primary biliary cirrhosis. *Biochim Biophys Acta* 2003; **1637**: 142–50.
3. Jungst C, Cheng B, Gehrke R, *et al.* Oxidative damage is increased in human liver tissue adjacent to hepatocellular carcinoma. *Hepatology* 2004; **39**: 1663–72.
4. Blackburn EH. Structure and function of telomeres. *Nature* 1991; **350**: 569–73.
5. Levy MZ, Allsopp RC, Futcher AB, *et al.* Telomere end-replication problem and cell aging. *J Mol Biol* 1992; **225**: 951–60.
6. Blackburn EH. Switching and signaling at the telomere. *Cell* 2001; **106**: 661–73.
7. Saretzki G, Von Zglinicki T. Replicative aging, telomeres, and oxidative stress. *Ann NY Acad Sci* 2002; **959**: 24–9.
8. Kurz DJ, Decary S, Hong Y, *et al.* Chronic oxidative stress compromises telomere integrity and accelerates the onset of senescence in human endothelial cells. *J Cell Sci* 2004; **117**: 2417–26.
9. Wiemann SU, Satyanarayana A, Tsahuridu M, *et al.* Hepatocyte telomere shortening and senescence are general markers of human liver cirrhosis. *FASEB J* 2002; **16**: 935–42.
10. Aikata H, Takaishi H, Kawakami Y, *et al.* Telomere reduction in human liver tissues with age and chronic inflammation. *Exp Cell Res* 2000; **256**: 578–82.
11. Oh BK, Jo Chae K, Park C, *et al.* Telomere shortening and telomerase reactivation in dysplastic nodules of human hepatocarcinogenesis. *J Hepatol* 2003; **39**: 786–92.
12. Desmet VJ, Gerber M, Hoofnargle JH, *et al.* Classification of chronic hepatitis: diagnosis, grading and staging. *Hepatology* 1994; **19**: 1513–20.
13. Kato J, Kobune M, Nakamura T, *et al.* Normalization of elevated hepatic 8-hydroxy-2′-deoxyguanosine levels in chronic hepatitis C patients by phlebotomy and low iron diet. *Cancer Res* 2001; **61**: 8697–702.
14. Hisatomi H, Nagao K, Kanamaru T, *et al.* Levels of telomerase catalytic subunit mRNA as a predictor of potential malignancy. *Int J Oncol* 1999; **14**: 727–32.
15. Kawakami Y, Kitamoto M, Nakanishi T, *et a l.* Immunohistochemical detection of human telomerase reverse transcriptase in human liver tissues. *Oncogene* 2000; **19**: 3888–93.
16. Moriguchi M, Nakajima T, Kimura H, *et al.* The copper chelator trientine has an antiangiogenic effect against hepatocellular carcinoma, possibly through inhibition of interleukin-8 production. *Int J Cancer* 2002; **102**: 445–52.
17. Nakajima T, Katagishi T, Moriguchi M, *et al.* Tumor size-independence of telomere length indicates an aggressive feature of HCC. *Biochem Biophys Res Commun* 2004; **325**: 1131–5.
18. Meeker AK, Gage WR, Hicks JL, *et al.* Telomere length assessment in human archival tissues: combined telomere fluorescence *in situ* hybridization and immunostaining. *Am J Pathol* 2002; **160**: 1259–68.
19. Iwama H, Ohyashiki K, Ohyashiki JH, *et al.* Telomeric length and telomerase activity vary with age in peripheral blood cells obtained from normal individuals. *Hum Genet* 1998; **102**: 397–402.
20. Kang SS, Kwon T, Kwon DY, Do SI. Akt protein kinase enhances human telomerase activity through phosphorylation of telomerase reverse transcriptase subunit. *J Biol Chem* 1999; **274**: 13085–90.
21. Kimura A, Ohmichi M, Kawagoe J, *et al.* Induction of hTERT expression and phosphorylation by estrogen via Akt cascade in human ovarian cancer cell lines. *Oncogene* 2004; **23**: 4505–15.
22. Haas-Kogan D, Shalev N, Wong M, *et al.* Protein kinase B (PKB/Akt) activity is elevated in glioblastoma cells due to mutation of the tumor suppressor PTEN/MMAC. *Curr Biol* 1998; **8**: 1195–8.
23. Wu SK, Wang BJ, Yang Y, *et al.* Expression of PTEN, PPM1A and P-Smad2 in hepatocellular carcinomas and adjacent liver tissues. *World J Gastroenterol* 2007; **13**: 4554–9.
24. Seki S, Kitada T, Yamada T, *et al. In situ* detection of lipid peroxidation and oxidative DNA damage in non-alcoholic fatty liver diseases. *J Hepatol* 2002; **37**: 56–62.
25. Ichiba M, Maeta Y, Mukoyama T, *et al.* Expression of 8-hydroxy-2′-deoxyguanosine in chronic liver disease and hepatocellular carcinoma. *Liver Int* 2003; **23**: 338–45.
26. Szatrowski TP, Nathan CF. Production of large amounts of hydrogen peroxide by human tumor cells. *Cancer Res* 1991; **51**: 794–8.
27. Toyokuni S, Okamoto K, Yodoi J, Hiai H. Persistent oxidative stress in cancer. *FEBS Lett* 1995; **358**: 1–3.
28. Chandel NS, McClintock DS, Feliciano CE, *et al.* Reactive oxygen species generated at mitochondrial complex III stabilize hypoxia-inducible factor-1alpha during hypoxia: a mechanism of O_2 sensing. *J Biol Chem* 2000; **275**: 25130–8.
29. Maulik N. Redox signaling of angiogenesis. *Antioxid Redox Signal* 2002; **4**: 805–15.
30. Sekoguchi S, Nakajima T, Moriguchi M, *et al.* Role of cell-cycle turnover and oxidative stress in telomere shortening and cellular senescence in patients with chronic hepatitis C. *J Gastroenterol Hepatol* 2007; **22**: 182–90.
31. Nakajima T, Moriguchi M, Katagishi T, *et al.* Premature telomere shortening and impaired regenerative response in hepatocytes of individuals with NAFLD. *Liver Int* 2006; **26**: 23–31.
32. Nagao K, Tomimatsu M, Endo H, *et al.* Telomerase reverse transcriptase mRNA expression and telomerase activity in hepatocellular carcinoma. *J Gastroenterol* 1999; **34**: 83–7.
33. Miura N, Shiota G, Nakagawa T, *et al.* Sensitive detection of human telomerase reverse transcriptase mRNA in the serum of patients with hepatocellular carcinoma. *Oncology* 2003; **64**: 430–4.
34. Kraemer K, Fuessel S, Schmidt U, *et al.* Antisense-mediated hTERT inhibition specifically reduces the growth of human bladder cancer cells. *Clin Cancer Res* 2003; **9**: 3794–800.

35. Cao Y, Li H, Deb S, Liu JP. TERT regulates cell survival independent of telomerase enzymatic activity. *Oncogene* 2002; **21**: 3130–8.
36. Liu DY, Peng ZH, Qiu GQ, Zhou CZ. Expression of telomerase activity and oxidative stress in human hepatocellular carcinoma with cirrhosis. *World J Gastroenterol* 2003; **9**: 1859–62.
37. Liu K, Hodes RJ, Weng NP. Cutting edge: telomerase activation in human T lymphocytes does not require increase in telomerase reverse transcriptase (hTERT) protein but is associated with hTERT phosphorylation and nuclear translocation. *J Immunol* 2001; **166**: 4826–30.
38. Dong-Yun S, Yu-Ru D, Shan-Lin L, *et al.* Redox stress regulates cell proliferation and apoptosis of human hepatoma through Akt protein phosphorylation. *FEBS Lett* 2003; **542**: 60–4.
39. Leslie NR, Bennett D, Lindsay YE, *et al.* Redox regulation of PI 3-kinase signalling via inactivation of PTEN. *EMBO J* 2003; **22**: 5501–10.
40. Shiota G, Maeta Y, Mukoyama T, *et al.* Effects of Sho-Saiko-to on hepatocarcinogenesis and 8-hydroxy-2′-deoxyguanosine formation. *Hepatology* 2002; **35**: 1125–33.
41. Wada S, Satomi Y, Murakoshi M, *et al.* Tumor suppressive effects of tocotrienol *in vivo* and *in vitro*. *Cancer Lett* 2005; **229**: 181–91.
42. Nishikawa T, Nakajima T, Moriguchi M, *et al.* A green tea polyphenol, epigalocatechin-3-gallate, induces apoptosis of human hepatocellular carcinoma, possibly through inhibition of Bcl-2 family proteins. *J Hepatol* 2006; **44**: 1074–82.
43. Naasani I, Oh-Hashi F, Oh-Hara T, *et al.* Blocking telomerase by dietary polyphenols is a major mechanism for limiting the growth of human cancer cells *in vitro* and *in vivo*. *Cancer Res* 2003; **63**: 824–30.
44. Tauchi T, Nakajima A, Sashida G, *et al.* Inhibition of human telomerase enhances the effect of the tyrosine kinase inhibitor, imatinib, in BCR–ABL-positive leukemia cells. *Clin Cancer Res* 2002; **8**: 3341–7.

Hepatology Research 2009; **39**: 366–373 doi: 10.1111/j.1872-034X.2008.00464.x

Original Article

Analysis of hepatic genes involved in the metabolism of fatty acids and iron in nonalcoholic fatty liver disease

Hironori Mitsuyoshi[1], Kohichiroh Yasui[1], Yuichi Harano[2], Mio Endo[1], Kazuhiro Tsuji[1], Masahito Minami[1], Yoshito Itoh[1], Takeshi Okanoue[3] and Toshikazu Yoshikawa[1]

[1]Molecular Gastroenterology and Hepatology, Graduate School of Medical Science, Kyoto Prefectural University of Medicine, Kyoto, [2]Department of Hepatology, Akashi City Hospital, Akashi, [3]Saiseikai Suita Hospital, Suita, Japan

Aims: Hepatic steatosis and iron cause oxidative stress, thereby progressing steatosis to steatohepatitis. We quantified the expression of genes involved in the metabolism of fatty acids and iron in patients with nonalcoholic fatty liver disease (NAFLD).

Methods: The levels of transcripts for the following genes were quantified from biopsy specimens of 74 patients with NAFLD: thioredoxin (Trx), fatty acid transport protein 5 (FATP5), sterol regulatory element-binding protein 1c (SREBP1c), fatty acid synthase (FASN), acetyl-coenzyme A carboxylase (ACAC), peroxisome proliferative activated receptor α (PPARα), cytochrome P-450 2E1 (CYP2E1), acyl-coenzyme A dehydrogenase (ACADM), acyl-coenzyme A oxidase (ACOX), microsomal triglyceride transfer protein (MTP), transferrin receptor 1 (TfR1), transferrin receptor 2 (TfR2) and hepcidin. Twelve samples of human liver RNA were used as controls. Histological evaluation followed the methods of Brunt.

Results: The levels of all genes were significantly higher in the NAFLD patients than in controls. The Trx level increased as the stage progressed. The levels of FATP5, SREBP1c, ACAC, PPARα, CYP2E1, ACADM and MTP significantly decreased as the stage and grade progressed ($P < 0.05$). Hepatic iron score (HIS) increased as the stage progressed. The TfR1 level significantly increased as the stage progressed ($P < 0.05$), whereas TfR2 level significantly decreased ($P < 0.05$). The ratio of hepcidin mRNA/ferritin ($P < 0.001$) or hepcidin mRNA/HIS ($P < 0.01$) was significantly lower in NASH patients than simple steatosis patients.

Conclusions: Steatosis-related metabolism is attenuated as NAFLD progresses, whereas iron-related metabolism is exacerbated. Appropriate therapies should be considered on the basis of metabolic changes.

Key words: fatty acids, iron, NAFLD, oxidative stress

Abbreviations
Trx, thioredoxin; FATP5, fatty acid transport protein 5; SREBP1c, sterol regulatory element-binding protein 1c; FASN, fatty acid synthase; ACAC, acetyl-coenzyme A carboxylase; PPARα, peroxisome proliferative activated receptor α; CYP2E1, cytochrome P-450 2E1, ACADM, acyl-coenzyme A dehydrogenase; ACOX, acyl-coenzyme A oxidase; MTP, microsomal triglyceride transfer protein; TfR1, transferrin receptor 1, TfR2, transferrin receptor 2.

INTRODUCTION

NON ALCOHOLIC FATTY liver disease (NAFLD) is a wide-spectrum liver disease, ranging from simple steatosis to steatohepatitis.[1] Owing to the obesity epidemic, NAFLD is now recognized as a leading health problem worldwide.[1] Since NAFLD has been documented to progress to liver failure[2] and/or hepatocellular carcinoma,[3] various therapeutic studies for NAFLD or nonalcoholic steatohepatitis (NASH) have been conducted to date.[4–8] These studies included weight reduction,[4] use of insulin sensitizers,[5] antioxidants,[6] phlebotomy[7] and hepato-protective drugs,[8] albeit with limited success. Although these treatments are aimed at addressing the pathogenesis of NAFLD, they would not always be efficient at every stage of this "wide spectrum" disease.

NASH is thought to develop through a "two-hit theory".[9] The first hit includes insulin resistance, mostly due to obesity.[9] The second hits include oxidative stress, inflammatory cytokines, and bacterial endotoxin.[9] In particular, the accumulation of fatty acids in the liver results in oxidative stress through oxidation of fatty

Correspondence: Dr Hironori Mitsuyoshi, Molecular Gastroenterology and Hepatology, Graduate School of Medical Science, Kyoto Prefectural University of Medicine, Kawaramachi Hirokouji, Kamigyo-ku, Kyoto 602-8566, Japan. Email: hmitsu@koto.kpu-m.ac.jp
Received 22 July 2008; revised 22 September 2008; accepted 1 October 2008.

acids.[10] In addition, hepatic iron load, which also induces oxidative stress, has been reported in some groups of patients with NAFLD.[11] Therefore, hepatic metabolism of fatty acids and iron should be the therapeutic target for NAFLD. However, their roles in the development of NAFLD have not yet been studied

In this study, we quantified the expression of genes involved in hepatic metabolism of fatty acids and iron using liver biopsy specimens from patients with NAFLD, and compared them with liver histology. Based on the results, we explored the role of the metabolism of fatty acids and iron in NAFLD. Our study should improve out understanding of the pathogenesis of NAFLD and contribute to the identification of putative therapeutic pathways.

PATIENTS AND METHODS

Patients

NAFLD PATIENTS WHO underwent liver biopsies in our institute between April 2000 and March 2007 were retrospectively selected according to the following criteria: no excessive alcohol intake (more than 20 g/day), as assessed by interview (on at least three occasions); no history of treatment with steatosis-inducing drugs within the 12 months prior to the study; negative serum hepatitis C virus (HCV) antibody; negative for hepatitis B surface antigen or antibodies to human immunodeficiency virus; and an absence of other forms of chronic liver disease, such as autoimmune liver diseases. Anthropometry and laboratory data were collected from all patients at the time of the liver biopsy. All patients had given written informed consent for the analysis of metabolic genes and liver biopsies before the study. The study protocol conformed to the ethical guidelines of the 1975 Declaration of Helsinki and was approved by the Ethics Committee of the Kyoto Prefectural University of Medicine.

Laboratory determinations

After a 12-h overnight fast, venous blood samples were drawn to determine asparatate aminotransferase (AST), alanine aminotransferase (ALT), albumin, total cholesterol, triglyceride, fasting plasma glucose (FPG), glycosylated haemoglobin (HbA_{1c}), insulin and ferritin levels. These parameters were measured using standard techniques from clinical chemistry laboratories. The index of insulin resistance was calculated only in patients without overt diabetes (fasting plasma glucose >126 mg/dL), according to the homeostasis model assessment (HOMA).

Histological evaluation

Formalin-fixed and paraffin-embedded liver biopsy specimens were stained with hematoxylin–eosin, Masson's trichrome, and Perl's Prussian blue. The stage of hepatic fibrosis was scored according to Brunt[12]: 1, zone 3 fibrosis; 2, zone 3 fibrosis with periportal fibrosis; 3, bridging fibrosis; and 4, cirrhosis. The grade of inflammation was scored as follows[12]: 1, mild; 2, moderate; and 3, severe. We considered the scores of stage and grade of simple steatosis as "0". Steatosis was assessed according to the percentage of hepatocytes containing fat droplets. The degree of iron loading was graded using a Perl's score of 0–4, as described previously.[13]

Quantification of the expression of hepatic genes

Liver specimens were immediately frozen after the biopsy and were stored at −80°C until use. Total RNA was isolated from biopsy specimens using the RNeasy kit (Qiagen, Hilden, Germany). First-strand cDNA was obtained from total RNA using the QuantiTect Reverse Transcription kit (Qiagen). PCR was performed using the Light Cycler 2.0 System (Roche, Mannheim, Germany), and the mRNA levels were normalized to those of β-actin. Comprehensive target genes were as follows: thioredoxin (Trx), fatty acid transport protein 5 (FATP5), sterol regulatory element-binding protein 1c (SREBP1c), fatty acid synthase (FASN), acetyl-coenzyme A carboxylase (ACAC), peroxisome proliferative activated receptor α (PPARα), cytochrome P-450 2E1 (CYP2E1), acyl-coenzyme A dehydrogenase, C4 to C12 straight chain (ACADM), acyl-coenzyme A oxidase (ACOX), microsomal triglyceride transfer protein (MTP), transferrin receptor 1 (TfR1), transferrin receptor 2 (TfR2) and hepcidin. Table 1 summarizes the specific primers for these target genes. Twelve samples of human total liver RNA were obtained from commercial sources (Stratagene, CA, USA; Clontech Laboratories, CA, USA; Ambion, TX, USA; Becton, Dickinson, NJ, USA; Cell Applications, CA, USA), and used as controls.

Statistical analysis

Associations between variables were analyzed using the Spearman's correlation coefficient by rank. Differences between variables were analyzed using the Mann–Whitney U-test or Kruskal–Wallis test. All analyses were performed using SPSS software for Windows, version

Table 1 The specific primers used for the target genes

	Sense primers	Antisense primers
Trx	5′-CTGCTTTTCAGGAAGCCTTG-3′	5′-ACCCACCTTTTGTCCCTTCT-3′
FATP5	5′-ACACACTCGGTGTCCCTTTC-3′	5′-CTACAGGGCCCACTGTCATT-3′
SREBP1c	5′-TGCATTTTCTGACACGCTTC-3′	5′-CCAAGCTGTACAGGCTCTCC-3′
FASN	5′-TTCCGAGATTCCATCCTACG-3′	5′-TGTCATCAAAGGTGCTCTCG-3′
ACAC	5′-GAGAACTGCCCTTTCTGCAC-3′	5′-CCAAGCTCCAGGCTTCATAG-3′
PPARα	5′-GGAAAGCCCACTCTGCCCCCT-3′	5′-AGTCACCGAGGAGGGGCTCGA-3′
CYP2E1	5′-CCCAAAGGATATCGACCTCA-3′	5′-AGGGTGTCCTCCACACACTC-3′
ACADM	5′-TTGAGTTCACCGAACAGCAG-3′	5′-AGGGGGACTGGATATTCACC-3′
ACOX	5′-TGATGCGAATGAGTTTCTGC-3′	5′-AGTGCCACAGCTGAGAGGTT-3′
MTP	5′-CATCTGGCGACCCTATCAGT-3′	5′-GGCCAGCTTTCACAAAAGAG-3′
TfR1	5′-ATGCATTTTGCAGCAGTGAG-3′	5′-TCCAAAAGGCCCTACTCCTT-3′
TfR2	5′-GACCCTGCAGTGGGTGTACT-3′	5′-CAGTCGCTCGTCTCTCTCCT-3′
hepcidin	5′-ACCAGAGCAAGCTCAAGACC-3′	5′-AAACAGAGCCACTGGTCAGG-3′

Note: The role of genes analyzed in lipid and iron metabolisms is as follows: oxidative stress-induced, Trx; uptake of fatty acid, FATP5; synthesis of fatty acid, SREBP1c, FASN, ACAC, oxidation of fatty acid, PPARα, CYP2E1, ACADM, ACOX, secretion of triglyceride, MTP; uptake of transferrin-bound iron, TfR1, TfR2; regulation of iron metabolism, hepcidin.
Trx, thioredoxin; FATP5, fatty acid transport protein 5, SREBP1c, sterol regulatory element-binding protein 1c; FASN, fatty acid synthase; ACAC, acetyl-coenzyme A carboxylase; PPARα, peroxisome proliferative activated receptor α; CYP2E1, cytochrome P-450 2E1, ACADM, acyl-coenzyme A dehydrogenase; ACOX, acyl-coenzyme A oxidase; MTP, microsomal triglyceride transfer protein; TfR1, transferrin receptor 1, TfR2, transferrin receptor 2.

14.0 (SPSS, Chicago, IL, USA). A P value of less than 0.05 was considered significant.

RESULTS

The characteristics of patients

TABLES 2 AND 3 summarize the characteristics of patients and the results of liver histology, respectively. Of the 16 diabetic patients, 3 had been treated with metformin, 2 with pioglitazone, 2 with sulfonylurea, and the others had been followed with diet restriction. Serum triglyceride levels were greater in the simple steatosis patients than in the NASH patients. Although the values of HbA_{1c} were comparable in the two groups, those of HOMA-IR [index of insulin resistance (IR)] were significantly higher in the NASH

Table 2 Patients characteristics

	Simple steatosis ($n = 33$)	NASH ($n = 41$)	P value
Age	55.4 ± 15.0	61.2 ± 12.7	0.051
BMI (kg/m^2)	27.5 ± 2.4	26.5 ± 4.4	0.748
Sex (male/female)	24/9	25/16	0.208
Diabetes (yes/no)	7/26	9/32	0.584
Plt	21.6 ± 3.9	19.1 ± 6.3	0.006
AST	43.0 ± 21.4	72.9 ± 30.5	0.0002
ALT	62.3 ± 30.8	89.8 ± 50.3	0.006
Alb	4.7 ± 0.3	4.6 ± 0.3	0.023
T-Cho	231.1 ± 50.5	199.9 ± 44.0	0.006
TG	205.0 ± 105.8	140.9 ± 103.2	0.015
FPG	145.1 ± 68.4	116.7 ± 21.5	0.356
HbA_{1c}	6.6 ± 1.8	6.0 ± 0.6	0.533
HOMA-IR	2.9 ± 1.2	4.6 ± 1.8	0.012
ferritin	223.1 ± 106.0	197.7 ± 160.7	0.227

Note: The value is expressed as either mean ± S.D. or the number of patients.
ALT, alanine aminotransferase; AST, asparatate aminotransferase; Alb, albumin; BMI, body mass index; FPG, fasting plasma glucose; HbA_{1c}, glycosylated haemoglobin; HOMA-IR, homeostasis model assessment-index of insulin resistance; T-Cho, total cholesterol; TG, triglyceride.